S123 **Breakdown of ITCZ-like PV Patterns**

Ajay Raghavendra* and Thomas A. Guinn†
Embry-Riddle Aeronautical University, Daytona Beach, Florida

1. INTRODUCTION

The band of elongated convection called the Inter Tropical Convergence Zone (ITCZ) is observed to undulate and breakdown into smaller disturbances that may potentially evolve into tropical cyclones (TCs) (see Fig. 6). The dynamics associated with the breakdown of idealized ITCZ-like potential vorticity (PV) patterns have been previously investigated in numerous barotropic studies (*e.g.,* Guinn and Schubert, 1993; Ferreira and Schubert, 1997) as well as full physical model studies (*e.g.*, Wang and Magnusdottir, 2005). This paper expands the previous barotropic studies by introducing irregularities in the PV pattern representing observed irregularities in convective activity within the ITCZ (see Fig. 1). This study also investigated the effects of asymmetry on the evolution of PV strips of finite length again representing ITCZ-like structures. While the barotropic nature of the model is incapable of capturing all the processes such as moisture physics, they retain many of the fundamental dynamics.

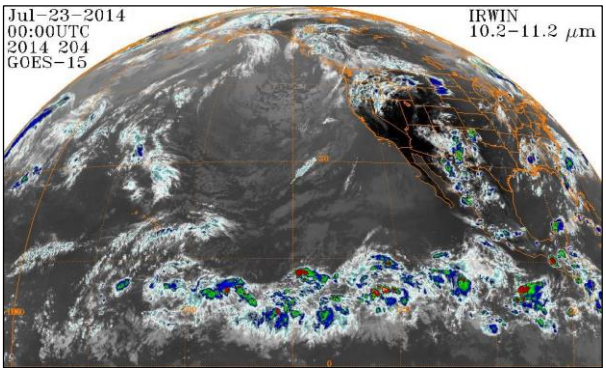

Fig. 1. A GOES 15 IR image of the ITCZ. The bright colors are indicative of non-uniform convection along the ITCZ.

This paper is organized as follows: Section 2 describes the shallow water equations (SWEs) and the numerical aspects of the model. A brief description of the mass sink has also been introduced in this section. Section 3 discusses the initial condition common to all six simulations presented in this paper followed by initial conditions unique to each simulation. Section 4 compares the results obtained from the six simulations. A summary of the model results followed by concluding remarks is presented in Section 5.

* *Corresponding author address*:
Ajay Raghavendra, Embry-Riddle Aeronautical Univ.,
Daytona Beach, FL 32114-3900. E-mail: ajay.rrs@gmail.com
† *Research advisor*

2. MODEL DESCRIPTION

A normal mode spectral model was developed to solve the SWEs in Cartesian coordinates on an f-plane (10˚ latitude) using a doubly periodic domain $0 \le x \le L_x, 0 \le y \le L_y$ where L_x and L_y represent the length and width of the model domain.

$$\frac{\partial u}{\partial t} - \left(f + \frac{\partial v}{\partial x} - \frac{\partial u}{\partial y}\right)v + \frac{\partial}{\partial x}\left[gh + \frac{1}{2}(u^2 + v^2)\right] = \kappa\nabla^2 u \quad (1)$$

$$\frac{\partial v}{\partial t} - \left(f + \frac{\partial v}{\partial x} - \frac{\partial u}{\partial y}\right)u + \frac{\partial}{\partial y}\left[gh + \frac{1}{2}(u^2 + v^2)\right] = \kappa\nabla^2 v \quad (2)$$

$$\frac{\partial h}{\partial t} + \frac{\partial (uh)}{\partial x} + \frac{\partial (vh)}{\partial y} = S + \kappa\nabla^2 h \quad (3)$$

In equations (1)-(3), u and v represent the zonal and meridional component of the velocity vector, respectively, g the acceleration due to gravity, f the Coriolis parameter, h the fluid depth, S the effects of convective heating (mass sources or sinks) and κ the diffusion constant.

The technique used solve equations (1)-(3) in the normal-mode method identical to Guinn (1992) and Guinn and Schubert (1993). All simulations were conducted on a 6,400km × 6,400km domain with 512 × 512 grid points. Time integration was performed using a fourth-order Adams-Bashforth-Moulton predictor-corrector scheme. The run time for each simulation was 120 hours with a 60s time step.

To prevent aliasing of quadratically non-linear terms, 170 waves were retained resulting in an effective horizontal resolution of approximately 37km. To reduce spectral blocking, ordinary diffusion was included i.e. $\kappa\nabla^2 u, \kappa\nabla^2 v$ and $\kappa\nabla^2 h$ on the right hand side of equations (1)-(3). The diffusion constant was chosen such that waves with total wavenumber 170 e-folded every 53 minutes.

The simulation of convection and resulting PV was achieved by introducing a mass sink in the continuity equation. In the shallow water framework, PV is given as:

$$PV = \frac{(\zeta + f)}{h} \ ,$$

where ζ is the relative vorticity, H is the mean fluid depth and h is the fluid depth.

To see the analogy between shallow water PV and Ertel's PV, consider the vertical contribution to Ertel's PV, which is

$$PV = \frac{1}{\rho}(\zeta + f)\frac{\partial \theta}{\partial z} \ ,$$

where ρ is the density of the fluid, ζ is the relative vorticity, f is the Coriolis parameter and θ is the potential temperature. Ertel's PV can be thought of as the absolute vorticity divided by the height difference between two θ-surfaces (z). In the real atmosphere, convection results in latent heat of condensation *i.e.,* diabatic heating increases the vertical θ gradient resulting in smaller distances between θ surfaces. In the shallow water framework this is closely analogous to shallower fluid depth. Therefore, convection can be simulated in a predetermined region by introducing a mass sink that locally decreases the mean fluid depth.

3. INITIAL CONDITIONS

Four variations of infinite strips and two finite strips (six cases in total) were developed to describe the initial distribution of vorticity in the domain (see 3.1-3.6 for the description of each case). Sharp gradients and discontinuities in the initial disturbance or mass sink result in model noise due to Gibbs phenomena. This problem is solved by describing our initial disturbances and sinks using piecewise continuous functions that were at least second order continuous. Following Shubert et.al (1999), a Hermite polynomial of the form $P(x) = 1 - 3x^2 + 2x^3$ where $x \in \{0, 1\}$ was used to smoothly transition the vorticity patterns from their maximum value at the perimeter of the strip to zero over a specified distance. This technique was also utilized to smoothly dampen the mass sink from the region of maximum heating to zero heating over a specified distance. Using the non-linear balance equation (*e.g.* Guinn and Schubert 1993 and DeMaria and Schubert, 1984; for a detailed explanation see Thelwell, 2001) the velocity and height fields were obtained from the initial vorticity field.

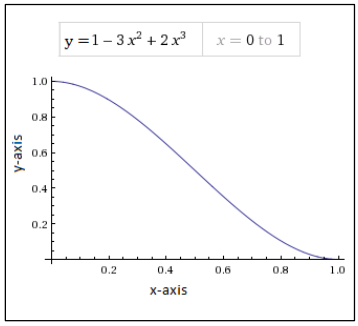

Fig. 2. Plot of the cubic Hermite Polynomial $P(x) = 1 - 3x^2 + 2x^3$. Note that $\frac{d}{dx}p(x) = 0 \; at \; x = 0 \; and \; 1$.

In general, if $p(a, b)$ describes the closed two dimensional perimeter of the initial vorticity field (where (a, b) represent the set of all points that lie on or inside the perimeter p) and, d is the outward perpendicular distance from $p(a, b)$ over which the cubic Hermite polynomial (Hr) smoothly decreases the vorticity from some constant value ζ_o to zero, the initial vorticity field is given by:

$$\zeta(x,y) = \begin{cases} \zeta_o \text{ if } \forall \{x,y\} \in \mathbb{R}^2, p(x,y) \in p(a,b) \\ \zeta_o \cdot Hr \\ \quad \text{if } \forall \{x,y\} \in \mathbb{R}^2, p(x,y) \in p(a,b) + d \\ \quad \text{and } p(x,y) \notin p(a,b) \\ \text{zero elsewhere} \end{cases}$$

Since the model is doubly-periodic in both x and y, the net circulation must be zero, which requires the domain-averaged vorticity be zero. This is achieved by creating the initial vorticity shape then zeroing the spectral coefficients corresponding to the mean (*i.e.*, wavenumbers zero). This introduces a weakly negative background vorticity field, which is minimized by using a larger than necessary model domain.

3.1 *Case 1*

An infinite strip 400km wide that includes the last 100km of each side of the strip gradually tapering to zero following the Hermite polynomial (see Fig. 2). The inner 200 km wide region is a strip of uniform vorticity of value $7.5\times10^{-5}s^{-1}$. This gives us a domain average vorticity of 3.515×10^{-5} s^{-1}. The results from this simple case served as a verification for the proper function of the model (*e.g.* Guinn, 1992; Guinn and Schubert, 1993; Ferreira and Schubert, 1997) and provided a foundation for all other comparisons. To accelerate the breakdown of the vortex pattern, a wave number 16 broadband perturbation (*e.g.* Schubert et al., 1999) with a magnitude of 0.3% of the maximum vorticity was added to the strip.

3.2 *Case 2*

Similar to Case 1 except the inner 200km wide region was a strip of uniform vorticity ($7.4\times10^{-5}s^{-1}$), and 10 circular regions of higher vorticity ($1.7\times10^{-5}s^{-1}$) with uniform spacing were embedded along the center of the strip. The radius of each circular region was 40km, and similar to the infinite strip, a Hermite polynomial is used to decrease the vorticity over an additional 40km. To effectively study the variations in PV rearrangement of various strips, calculations were made to ensure the domain average vorticity of this disturbance is similar to Case 1.

3.3 *Case 3*

Identical to Case 2 except the 10 circular regions of higher vorticity were randomly spaced near the center of the strip. There also exists up to a ±10% random variation in the magnitude of the vorticity in each circular regions of higher vorticity.

3.4 *Case 4*

Identical to Case 1 except there was no broadband perturbation and ten uniform linearly spaced circular mass sinks were positioned along the center of the strip. The individual mass sinks each had a radius 40km with a Hermite polynomial used to decrease the magnitude of the sink over an additional 40km. The

shape of the circular sinks, $Q(x,y)$, followed the same format as the shape of the vorticity pockets in case 3 and as shown in Fig. 3. At its peak value, fluid was drained at the rate of 0.017ms^{-1} to simulate heating of 10K per day. Figure 4 shows the time profile of the sink. In this simulation, the sink was initiated at 0hrs, achieved its peak value at 12hrs, maintained peak heating over the next 6hrs and decreased to zero over an additional 12hrs. The sink was active for a total of 30hrs. The mathematical functions used to achieve such variations in the mass sinks were given by:

$$S(x,y,t) = \begin{cases} Q(x,y)\, e^{a(t-t_2)} \text{ if } t_1 \le t \le t_2 \\ Q(x,y) \text{ if } t_2 < t \le t_3 \\ Q(x,y)\, e^{-a(t-t_3)} \text{ if } t > t_3 \end{cases}$$

where, t_1, t_2 and t_3 represent the time at which the sink was turned on, maintained at a steady state and started to decrease respectively.

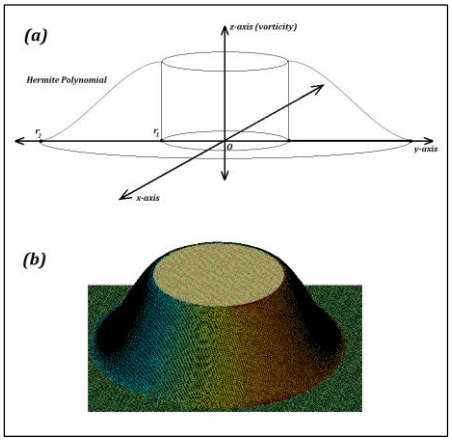

Fig. 3. Visualizing a pocket of vorticity in Case 2 and 3 of this section. (a) A sketch of the vortex pocket that consists of concentric cylinders of radii r_1 and r_2 and, the Hermite Polynomial smoothly reducing the value of vorticity over a radial distance from r_1 to r_2. (b) A 3D plot of the packet of vorticity.

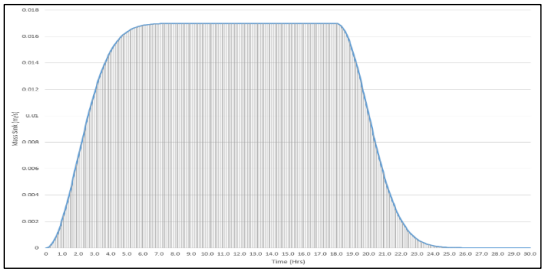

Fig. 4. Time variation of the heating function for Case 4

3.5 *Case 5*

This shape was a modification to Vaughan and Guinn (2013) where a symmetric "twinkie"-shaped finite strip of PV was studied. The motivation to study the asymmetric "twinkie"-shaped PV field stems from its climatological persistence (*e.g.* Waliser and Gautier, 1993 and Salby, 1991) and visual similarities to the ITCZ observed near the tropical eastern pacific. The time lapse diagrams in Fig. 7 provides an example of the reoccurring ITCZ pattern unique of the eastern Pacific region.

The lopsided "twinkie"-shape can be described as follows: the centers of two circles of radii 500km and 100km are separated by a distance of 2800km. Two exterior tangent lines connect the circles. The resulting outer perimeter describes the shape of the initial vorticity field (see Fig. 5). Similar to the previous initial conditions, a Hermite Polynomial smoothly reduces the value of vorticity from the peak value of 5.85×10^{-5}s^{-1} to zero over a distance of 100 km. The area average vorticity is equal to Case 1.

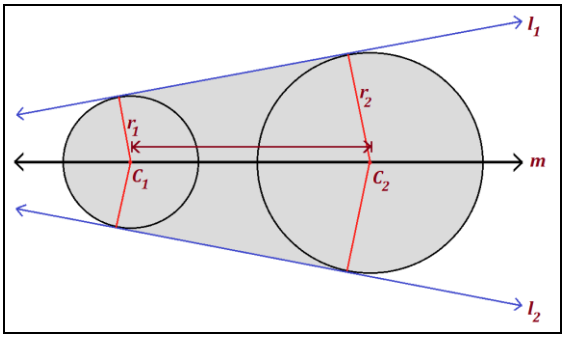

Fig. 5. Illustration of the lopsided Twinkie shape. Two circles with centers C_1 and C_2 and radii R_1 and R_2 separated by a distance "d". The shape of the initial vorticity field takes the form of the shaded portion in the above figure. Similar to other disturbances, a cubic-Hermite polynomial is used to gradually weaken the strength of the vorticity over a predetermined distance.

3.6 *Case 6*

A finite "twinkie"-shaped strip of vorticity similar to Vaughan and Guinn (2013). This case helps in making a comparison to case 5. The area of the strip and domain average vorticity is equal to case 5.

4. RESULTS

The evolution and breakdown of the three infinite strips carry subtle differences while on the other hand, the breakdown of the finite strips is differs significantly from each other. The differences in the results from the 6 cases are documented in this section. Please refer to Fig. 8-13 for illustrations showing the time evolution of PV at 0, 24, 48, 72, 96 and 120 hrs. for all six cases.

4.1 *Case 1*

According to linear stability theory for an infinite strip of uniform vorticity, the wavelength of the most unstable mode is approximately 8 times the width of the strip (Rayleigh, 1945; Guinn and Schubert, 1993). For a uniform infinite strip of width 200km, 300km and 400km, linear theory predicts the strip to breakdown into

approximately 4, 2.$\bar{6}$ and 2 disturbances, respectively, for a domain length of 6,400km. However, as described in section 3.1, the infinite strips of vorticity are not piecewise continuous step functions in x as in the linear stability analyses performed by Rayleigh (1945). A step function in x of uniform vorticity and width 300km would produce an identical domain averaged vorticity to the infinite strips presented in Cases 1-4. It is therefore reasonable to expect 2 to 4 disturbances to develop with 3 disturbances being favored in the breakdown of the infinite strips presented in this paper (Fig. 8-11). The evolution of the PV is similar to Guinn and Schubert (1993).

4.2 *Case 2*

In spite of the higher pockets of vorticity embedded along the infinite strip, there is little difference in the evolution and re-arrangement of PV. The 10 pockets of higher PV are sheared into a single strip and the end result is very similar to that of Case 1 (Fig. 9). In fact, it was noted in trial simulations (not shown) that the breakdown of the strip was more sensitive to the broadband perturbation than the magnitude of the circular regions of higher vorticity.

4.3 *Case 3*

The random spacing of the pockets of vorticity resulted in non-uniform pooling of vorticity along the strip. This resulted in a tendency to breakdown into four disturbances. However, it was noted in simulations with longer run times that the strip eventually breaks down into three disturbances. Towards the end of the simulation (see Fig. 10), the forth disturbance is unable to develop, sheared and merges with the neighboring disturbances. The random spacing of the circular regions of higher vorticity did little to alter the evolution the strip.

4.4 *Case 4*

Despite the lack of a broadband perturbation, the evolution of the strip was very similar to Case 3 (Fig. 11). This also suggests that the steady generation of PV via the mass sink is a superior perturbation mechanism when compared to the circular regions of higher vorticity.

4.5 *Case 5*

The region with the larger pool of vorticity (eastern portion) is initially pushed north and later engulfs the strip tapering near the southwest. The lopsided PV shape is suggestive of the breakdown of the ITCZ and formation of TCs observed in the Eastern-Pacific. Similar to the satellite time lapse (Fig. 7) the thin tapering strip of vorticity extending from the center of circulation shows little movement. This case also suggests barotropic processes are important in the evolution and breakdown of the ITCZ. By noting the difference in evolution between Case 5 and 6, we can conclude the shape of the finite strip also plays a key role in determining the end result.

4.6 *Case 6*

The breakdown of the finite strip is similar to Vaughan and Guinn (2013) for the same length to width ratio. Given the symmetry of the strip and nature of the numerical model, the strip broke down into two pools of uniform vorticity. It is interesting to note that in multiple variations of Case 5 (lopsided strips), no such split was observed.

5. SUMMARY AND CONCLUSIONS

It is noteworthy to mention the following quote by S. G. H. Philander et al. (1996)

> "*The most complex models are capable of the greatest realism, but their results are difficult to analyze explain. It is therefore important to have simpler models that by excluding certain processes, sacrifice realism, but in return allow detailed analysis and yield physical insight into the retaining processes*"

While the normal mode barotropic model with and f-plane approximation is unable to serve as a reliable forecasting tool, it offers excellent insight from a theoretical standpoint and is still prevalent in understanding TC dynamics (*e.g.* Hendricks et al., 2014). Given the barotropic nature of the tropics, the SWEs are capable of capturing many of the larger scale dynamics (*e.g.* Case 5) and offer meaningful insights with regard to the underlying dynamics.

One of the objectives of this project was to develop a normal-mode spectral model in a new generation user-friendly programing language that can be used for both education and research. The Fast Fourier Transform and matrix manipulation methods in Mathwork's MATLAB made it an ideal choice for this research project and future research work. Please contact the author if you are interested in obtaining a copy of the MATLAB scripts used for this project.

Acknowledgment

We would like to thank The Office of Undergraduate Research (IGNITE), Embry-Riddle Aeronautical University for funding this research project.

REFERENCES

DeMaria, M., and Schubert W. H., 1984: Experiments with a Spectral Tropical Cyclone Model. *J. Atmos. Sci.*, **41**, 901–924.

Guinn, T. A., and Schubert W. H., 1993: Hurricane spiral bands. *J. Atmos. Sci.*, **50**, 3380–3403.

Guinn, T. A., 1992: A dynamical theory for hurricane spiral bands. Ph.D. dissertation, Dept. of Atmospheric Science, Colorado State University, 178 pp.

Hendricks, E. A., W. H. Schubert, Y.-H. Chen, H.-C. Kuo, and M. S. Peng (2014), Hurricane eyewall evolution in a forced shallow water model,
J. Atmos. Sci., **71**, 1623–1643

Nieto Ferreira, R., and Schubert W. H., 1997: Barotropic aspects of ITCZ breakdown. *J. Atmos. Sci.*, **54**, 261–285.

Rayleigh, J. W. S., 1945: Vortex Motion and Sensitive Jets, *The Theory of Sound, Vol 2*, Dover Publications, 376-414.

Salby, M. L., Hendon, H. H., Woodberry, K, and Tanaka, K, 1991: Analysis of Global Cloud Imagery from Multiple Satellites. *Bull. Amer. Meteor. Soc.*, **72**, 467–480.

Schubert, W. H., M. T. Montgomery, R. K. Taft, T. A. Guinn, S. R. Fulton, J. P. Kossin, J. P. Edwards, 1999: Polygonal eyewalls, asymmetric eye contraction, and potential vorticity mixing in hurricanes. *J. Atmos. Sci.*, **56**, 1197-1223.

S. G. H. Philander, D. Gu, G. Lambert, T. Li, D. Halpern, N-C. Lau, and R. C. Pacanowski, 1996: Why the ITCZ Is Mostly North of the Equator. *J. Climate*, **9**, 2958–2972.

Thelwell, R, 2001: The Nonlinear Balance Equation: a Survey of Numerical Methods. Master's Thesis, Colorado State University.

Vaughan, M. T and Guinn, T. A., 2013: The Evolution of Finite Vorticity Strips using a Non-Divergent Barotropic Model. 12th Annual Student Conference, Austin, TX, Amer. Meteor. Soc., S68. [Available online at *https://ams.confex.com/ams/93Annual/webprogram/Paper224776.html*.]

Wang, C. and Magnusdottir, G., 2005: ITCZ Breakdown in Three-Dimensional Flows. *J. Atmos. Sci*., **62**, 1497–1512.

Waliser, D. E., and Gautier, C, 1993: A Satellite-derived Climatology of the ITCZ. *J. Climate*, **6**, 2162–2174.

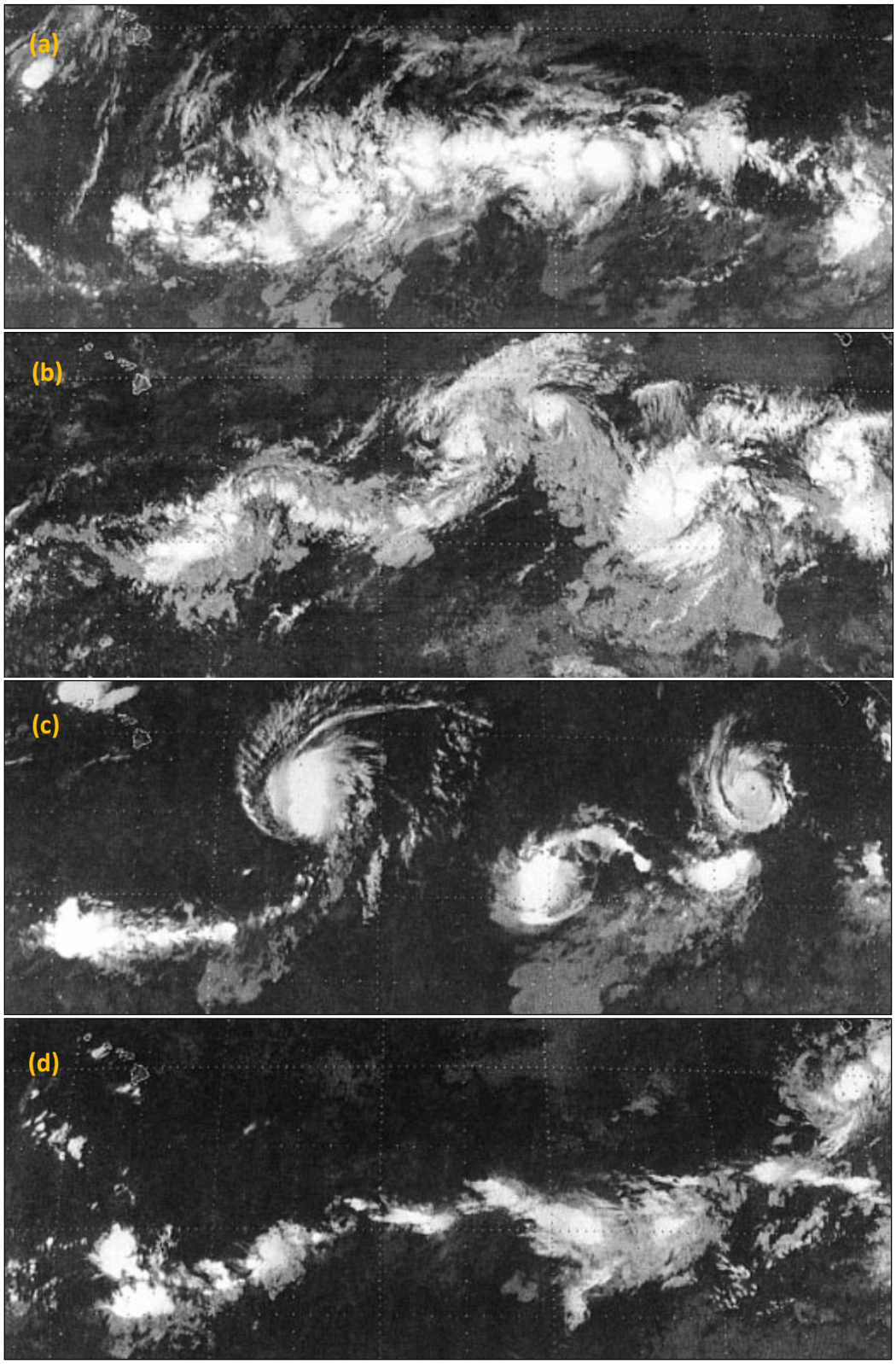

Fig. 6. GOES IR images at 1646 UTC on (a) 26 July, (b) 28 July, (c) 3 August, and (d) 12 August 1988 showing a case of ITCZ breakdown. Credit to Ferreira and Schubert (1997)

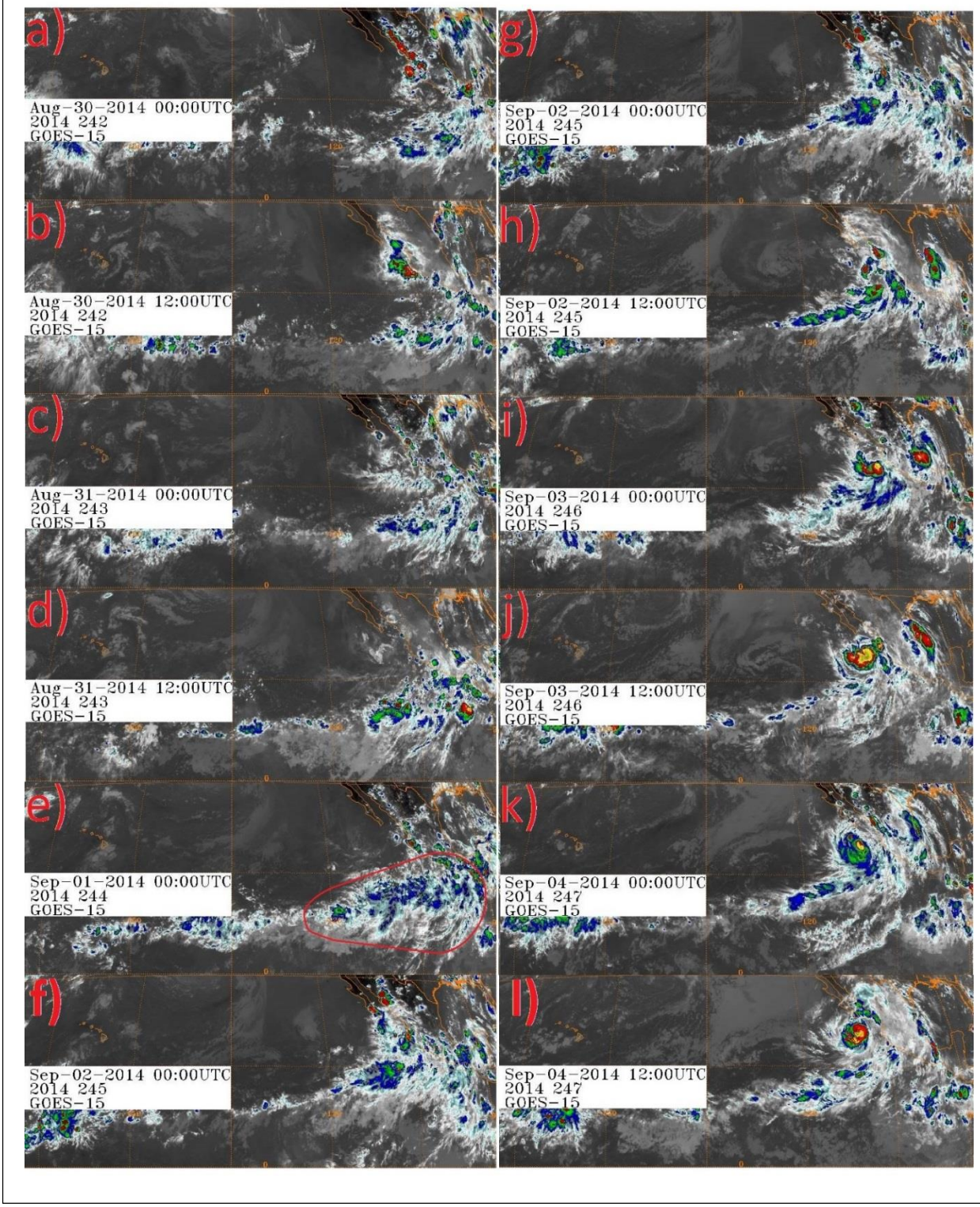

Fig. 7. A Time Lapse of an ITCZ Breakdown occurring between 30 Aug and 4 Sep 2014. GOES-15 IR images at 0000 UTC and 1200 UTC between 30-August and 4-September-2014 showing a case of ITCZ breakdown in the Eastern-Pacific.

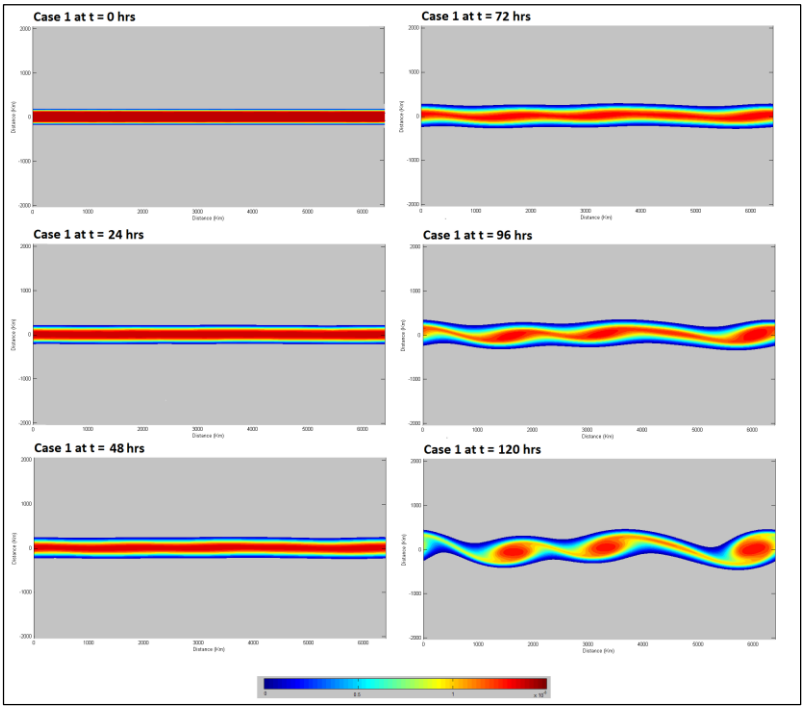

Fig. 8. Case 1: PV evolution of an infinite strip 400km wide with a wavenumber 16 broadband perturbation.

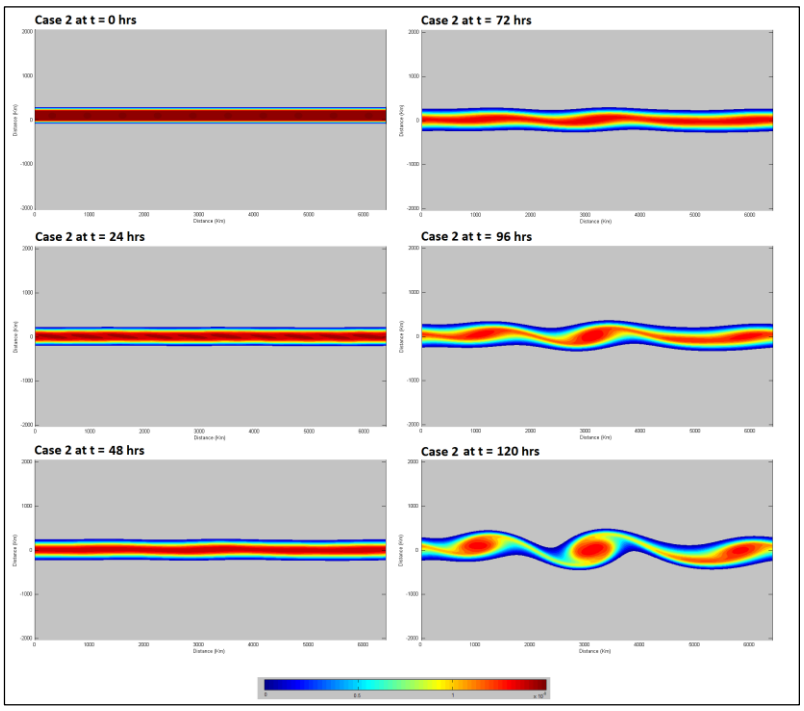

Fig. 9. Case 2: PV evolution of an infinite strip 400km wide with 10 circular uniform spacing regions of higher PV embedded along the center of the strip.

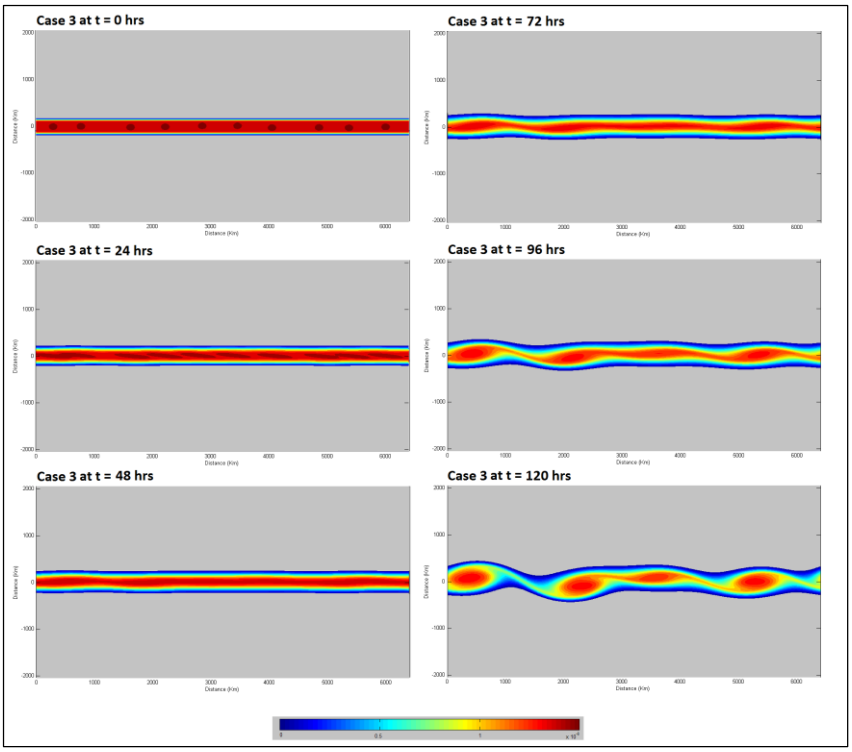

Fig. 10. Case 3: PV evolution of an infinite strip 400km wide with 10 circular randomly spaced regions of higher PV embedded near the center of the strip.

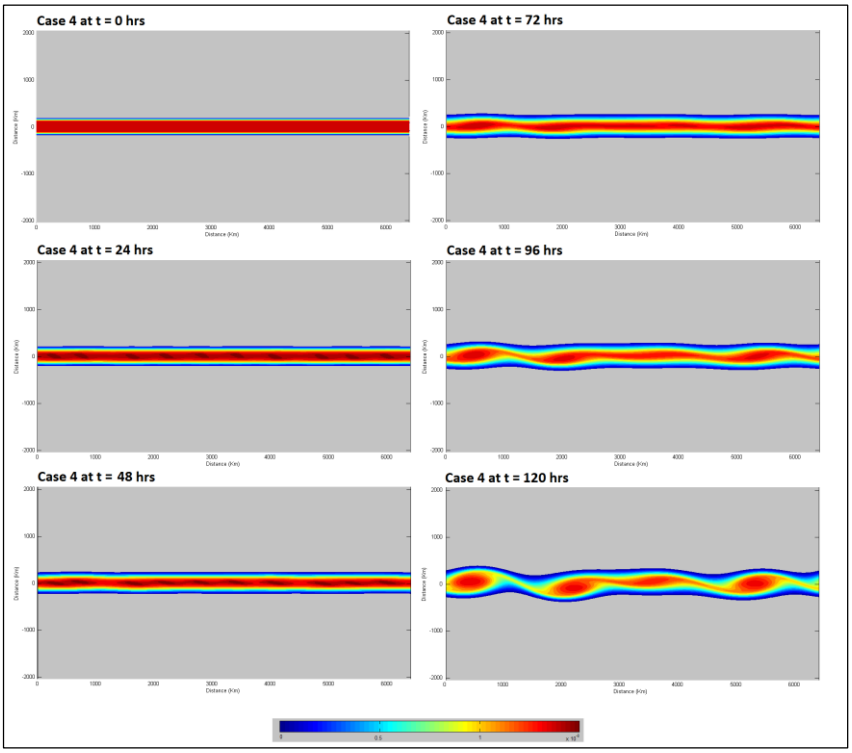

Fig. 11. Case 4: PV evolution of an infinite strip 400km wide with 10 circular uniformly spaced mass sinks along the center of the strip.

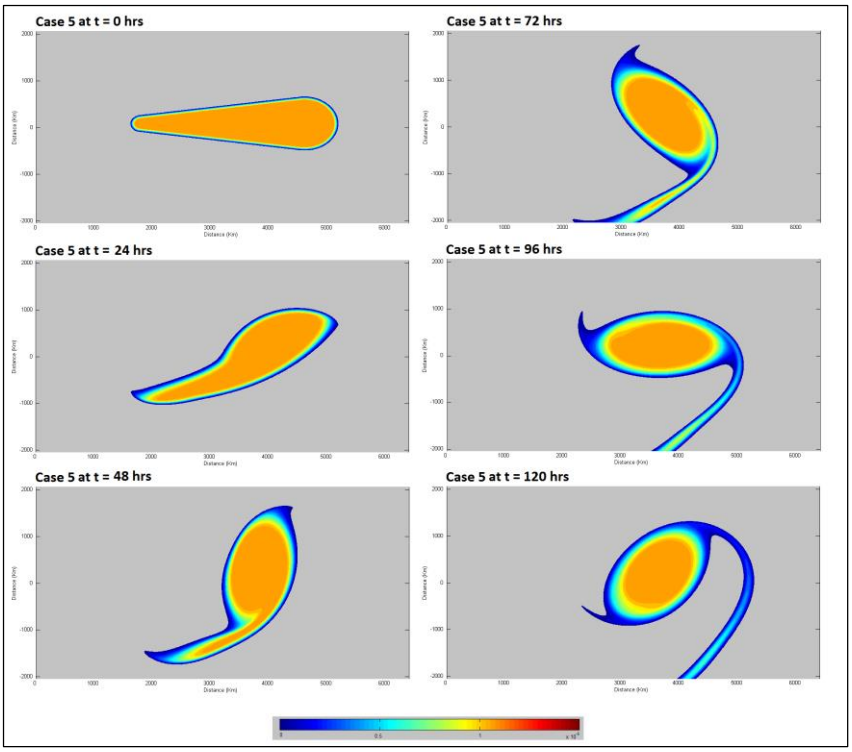

Fig. 12. Case 5: PV evolution of a finite non-uniform region of vorticity.

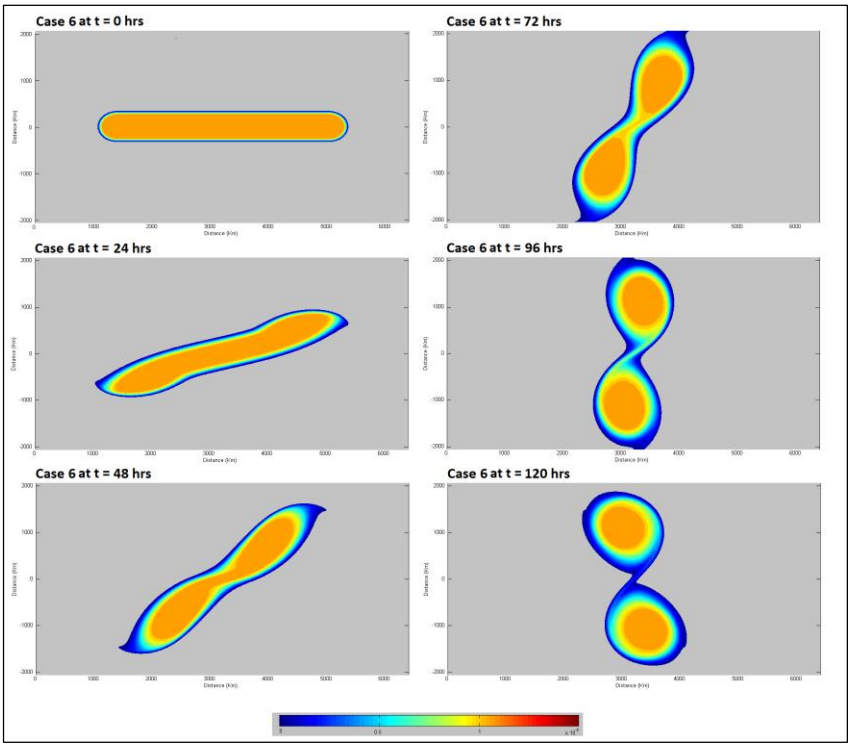

Fig. 13. Case 6: PV evolution of a finite uniform region of vorticity (Twinkie shape).